Enhancing photovoltaic performance of dye-sensitized solar cell by continual mesoporous TiO_2 films: Effects of annealing temperature and film thickness

B. YARMAND*
Nanotechnology and Advance Materials Department, Materials and Energy Research Center, Karaj, Iran

Continual mesoporous TiO_2 films were prepared by sol-gel templating technique as photoanodes of dye-sensitized solar cells. The effects of annealing temperature and film thickness were examined on the photovoltaic performance of solar cells. X-ray diffraction (XRD) analysis revealed that anatase phase was crystallized at 300 °C with initially crystallite size 3.2 nm and the crystallization was improved to 700 °C. Surface area analysis showed that the specific surface area of the films decreased from 163.43 to 87.15 m^2/g and the mean pore size increased from 5.05 to 8.75 nm as the annealing temperature increased from 400 to 600 °C. Transmission electron microscope (TEM) images proved that deposited films had nanostructured and mesoporous morphology. The transmittance spectra that measured by UV/Vis spectrophotometer revealed that the transmittance maxima of the films decreased in the visible region and the absorption edges shifted to longer wavelengths. Photovoltaic measurements showed that the power conversion efficiency of the films annealed at 400 °C initially enhanced to the maximum value of 3.61 % with the increasing film thickness to 1.7 μm and then declined when the film thickness increased further. By increasing annealing temperature to 600 °C the power conversion efficiency decreased to 2.94 %.

(Received March 22, 2014; accepted November 13, 2014)

Keywords: Dye-sensitized solar cell, TiO_2, Continual mesoporous films, Sol-gel templating process

1. Introduction

Dye-sensitized solar cells (DSSCs), since they were introduced by Gratzel in 1991 for the first time, have attracted a lot of attention as one of the best candidates for the next generation of solar cells. The reason is that the cost of producing these cells is low and they have much less environmental impact than conventional solid-state junction solar cells [1-3]. Photovoltaic performance of DSSCs is affected by physical and chemical properties of the materials which are used in making their components specially photoanodes. In photoanodes made of TiO_2 films, phase composition, crystal structure, crystallite size, specific surface area, roughness and morphology have a great influence on the overall efficiency [4-6]. Using continual mesoporous structures in making the photoandes of DSSCs has a key role in improving their photovoltaic performance because these structures, on one hand, with high specific surface area adsorb a lot of dye molecules and result in injecting more electrons to the semiconductor conduction band. On the other hand, using continual mesoporous structures with their continuous pathway and the least inhibitors to electrons movement, leads to increasing the charge collection efficiency. Besides, uniform and continuous pores in the structure increase the diffusion of electrolyte carriers for faster reduction of oxidized dye molecules [7-10].

Sol-gel method can be considered as most influential technique for preparation of continual mesoporous structures. By tailoring the chemical composition of primary precursor and controlling variables, continual mesoporous products with high level chemical purity and good homogeneity can be obtained [11, 12]. A combination of the evaporation-induced self-assembly (EISA) using structure-directing polymer (template) with complexation of molecular inorganic species in precursor can be used to prepare the continual mesoporous films through sol-gel process [13, 14]. Making DSSCs from continual mesoporous TiO_2 films using sol-gel templating method not only improves overall efficiency but also lowers the cost of the constructing process, which from the beginning have been the most important difficulties in the progress of DSSCs development.

This work is mainly focused on studying the precise formation of continual mesoporous TiO_2 films through sol-gel method by using Pluronic P123 as template and also studying the structural, surface, morphological and optical properties of the films when annealing temperature

changes. At the end the effects of two important factors, which are annealing temperature and film thickness, on photovoltaic performance of DSSCs made by these films have been evaluated.

2. Experimental

2.1. Preparation of continual mesoporous TiO_2 films

Titanium tetraisopropoxide [Ti $(O{\cdot}i\text{-}C_3H_7)_4$] 98 % (Merck) was used as precursor; hydrochloric acid 32 % (Merck) as catalyst, non-ionic triblock copolymer surfactant Pluronic P123 [poly-(ethylene oxide) poly-(propylene oxide) poly-(ethylene oxide) EO_{20}–PO_{70}–EO_{20}] (Aldrich) as template and ethanol 99.9 % (Merck) as solvent. All as received chemicals were used in the experiments. Quartz slide and FTO substrates were applied for deposition of the layers.

Continual mesoporous TiO_2 films were prepared by self-assembly of the Pluronic P123 triblock copolymer surfactant in sol-gel solution. Room temperature stirring of 5 g titanium tetraisopropoxide with 3.2 g hydrochloric acid for 10 min resulted in hydrolysis to occur. The hydrolyzed sol was mixed with 1 g Pluronic P123 surfactant being dissolved in 21 g ethanol under stirring for 10 min at room temperature. Substrates were subsequently coated with spin coater at 2000 rpm for 30 s. The films were then aged at 10 °C for 24 h under controlled humidity of 65-75 %. The samples were finally annealed in a tube furnace at different temperatures ranging from 300 to 800 °C for 1 h under air with a heating rate of 1 °C/min. This procedure was repeated for thickening of films.

2.2. Fabrication of DSSCs

FTO substrate having sheet resistance of 10 Ω/□ (Solaronix) was used to make both the working and counter electrodes. Productions of photoanodes were carried out by deposition and treatment of continual mesoporous TiO_2 films onto FTO substrates for several times. For sensitization, photoanodes with warming temperature of 80-100 °C was immersed in 0.5 mM ethanolic solution of *cis*-diisothiocyanato-bis(2,2′-bipyridyl-4,4′-dicarboxylato) ruthenium(II) bis(tetrabutylammonium) (N719, Solaronix) and kept at room temperature for 72 h. The dye-adsorbed photoanode was then rinsed thoroughly with ethanol and subsequently dried. Pt catalysts as the counter electrode were prepared by spreading a drop of 10 mM H_2PtCl_6 in isopropanol on FTO substrate and heating it to 400 °C for 15 min under air ambient. The electrodes were spaced and sealed by 25 μm thick thermoplast hot-melting sealing foil (SX 1170-25, Solaronix). Finally, the iodolyte electrolyte consisted of 50 mM of tri-iodide in acetonitrile (AN 50, Solaronix) was injected into the cell by capillary forces through a hole drilled in the counter electrode. The hole was covered and sealed with a quickly solidifying epoxy polymer to prevent fluid-type electrolyte leakage. The cells had an active area of 0.25 cm^2.

2.3. Characterization and measurements

Phase identification and crystallite size of the films were examined by an X-ray diffractometer with Cu-K_α radiation and Ni filter operated at 40 kV and 30 mA (Philips, PW3710). The scanning range was from 20 to 80 ° with a scanning rate of 0.25 °/min. Surface area analysis of the films was evaluated through nitrogen adsorption/desorption isotherms (BELSORP II). The Brunauer–Emmet–Teller (BET) specific surface area was calculated from the linear part of the BET plot (P/P_0 = 0.05 – 0.35). The pore size distribution plots were obtained by using the Barret–Joyner–Halenda (BJH) model. The morphology of the films was observed using transmission electron microscope (Philips, CM200 FEG). The thickness of TiO_2 films was measured by Alpha-step profiler. The optical transmittance spectra of the films were recorded using a UV/Vis spectrophotometer (Perkin Elmer, Lambda 25) with a scanning rate of 60 nm/min in the wavelength range of 200 – 800 nm. Photovoltaic measurements were performed under 1 sun AM 1.5G simulated sun light using a solar simulator (luzchem) and a potentiostate/galvanostae (PGSTAT 302N, Autolab, Eco-Chemie).

3. Results and discussion

3.1. XRD analysis

Fig. 1 shows the XRD patterns of powders scraped from the continual mesoporous TiO_2 films annealed at different temperatures. It is found that the continual mesoporous TiO_2 film prepared at room temperature is amorphous. The anatase peaks appeared at 300 °C explaining the nucleation of anatase crystals and beginning of phase transition from amorphous to anatase phase. By increasing temperature from 300 to 700 °C, the intensities of the anatase peaks were increased corresponding to the crystallite improvement. It can be observed that rutile peaks with low intensities appear at 700 °C. This explains a transition from anatase to rutile phase. By increasing the temperature to 800 °C, the intensities of the anatase peaks decrease, while those of the rutile peaks enhance. The strongest peak observed for anatase and rutile phases at different temperatures are (101) 2θ=25.4° and (110) 2θ=27.4°, respectively. No peaks are observed that might confirm the presence of the brookite phase or other compounds like carbon-containing impurity phases.

The average crystallite size of the anatase phase in continual mesoporous TiO_2 films can be calculated from the XRD data by using Scherrer's equation [15]:

$$D = \frac{k\lambda}{B\cos\theta}$$

where D is the average crystallite size, λ is the applied X-ray wavelength (λ=1.5406 Å), k=0.90 which is a constant, θ is the diffraction angle in degree and B is the full width at half maximum (FWHM) of the diffraction peak observed in radians. Lattice strain of the anatase phase can be estimated from the full width at half maximum (FWHM) of mean peaks by using Hall's equation [15]:

$$B\cos\theta = \frac{k\lambda}{D} + 2\varepsilon\sin\theta$$

where ε is the lattice strain estimated from the slope of the curve Bcosθ vs. 2sinθ. The effect of annealing temperature on crystallite size and lattice strain of the anatase phase of continual mesoporous TiO_2 films are shown in Fig. 2. As the annealing temperature increases, the anatase crystallites continue to grow. The crystallite size of the anatase phase increases about six times from 3.2 to 19.6 nm as the annealing temperature increases from 300 to 700 °C. Continual mesoporous TiO_2 films have very small crystallite sizes. This results due to using Pluronic P123 as a template [14]. The anatase phase is under tensile strain. As the annealing temperature increase, the strain in the anatase phase decreases which is attributed to decrease in the lattice imperfections [16].

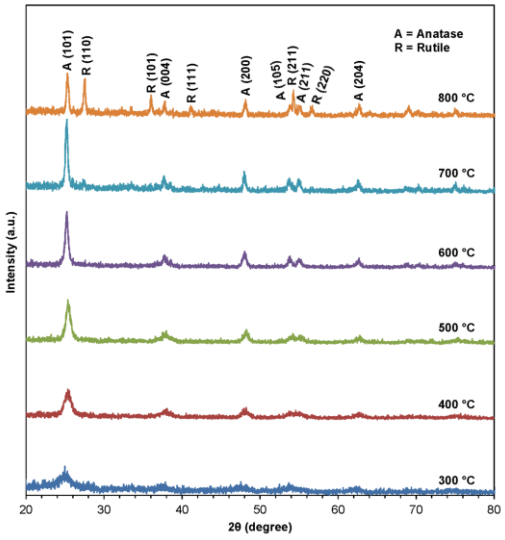

Fig. 1. XRD patterns of continual mesoporous TiO_2 films annealed at temperatures given in the figure.

3.2. BET and BJH analysis

The N_2 adsorption/desorption isotherms and BJH analysis of adsorption branches of powders scraped from the continual mesoporous TiO_2 films annealed at different temperatures are shown in Fig. 3. All isotherms show a type IV curve with H1 hysteresis loop that proves the TiO_2 films having mesoporous structure [17]. The BJH analysis shows narrow pore size distribution curves indicating mesoporous TiO_2 films having uniform pore channels. Variation of the specific surface area and pore size of the continual mesoporous TiO_2 films with the annealing temperature are shown in Table 1. It can be seen that by increasing the annealing temperature from 400 to 600 °C, the specific surface area decreases from 163.43 to 87.15 m^2/g, while the mean pore size increases from 5.05 to 8.75 nm. These changes in surface area and pore properties of the continual mesoporous TiO_2 films with the annealing temperature might be the result of crystallite growth and remove of small pores.

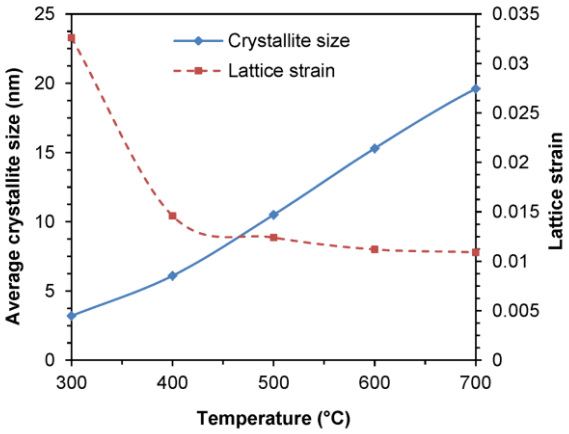

Fig. 2. Variation of crystallite size and lattice strain of anatase phase with the annealing temperature.

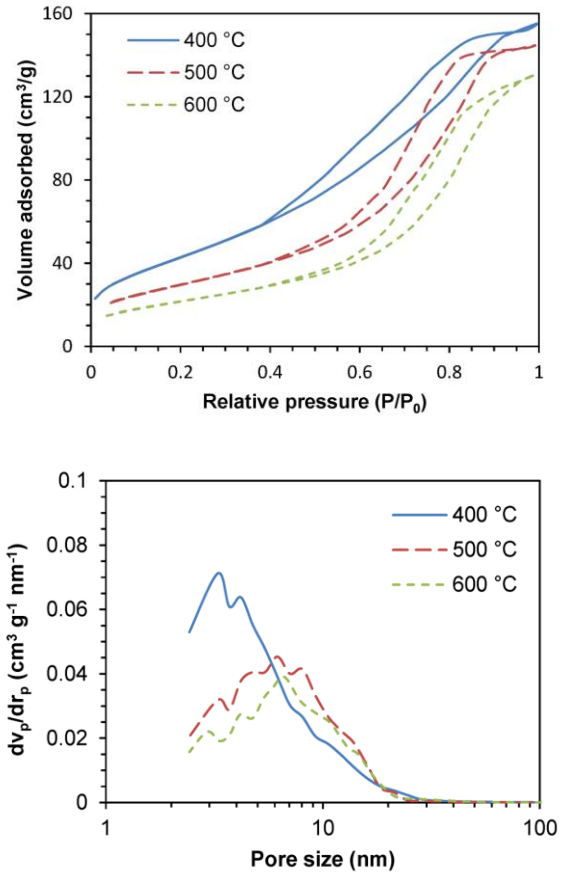

Fig. 3. N_2 adsorption/desorption isotherms and BJH pore size distribution of adsorption branches of continual mesoporous TiO_2 films at different temperatures.

Table 1. Specific surface area and pore size of continual mesoporous TiO_2 films annealed at different temperatures.

Annealing temperature (°C)	Specific surface area (m^2/g) [by BET]	Mean pore size (nm) [by BET]	Average pore size (nm) [by BJH, adsorption]	Average pore size (nm) [by BJH, desorption]
400	163.43	5.05	3.28	3.28
500	108.91	8.21	6.18	6.18
600	87.15	8.75	6.65	7.03

3.3. Morphological characterization

TEM is used to confirm the film continual mesoporous structure. Fig. 4 shows TEM images of the continual mesoporous TiO_2 film annealed at 400 °C. As seen in Fig. 4a, it can be concluded that anatase nanocrystals connect with each other to produce a framework consisting of the mesopores. Fig. 4b shows that anatase nanocrystals have diameters of about 5-7 nm and are randomly oriented. The selected area electron diffractogram exhibits rings with spots confirming the presence of very small anatase nanocrystallites.

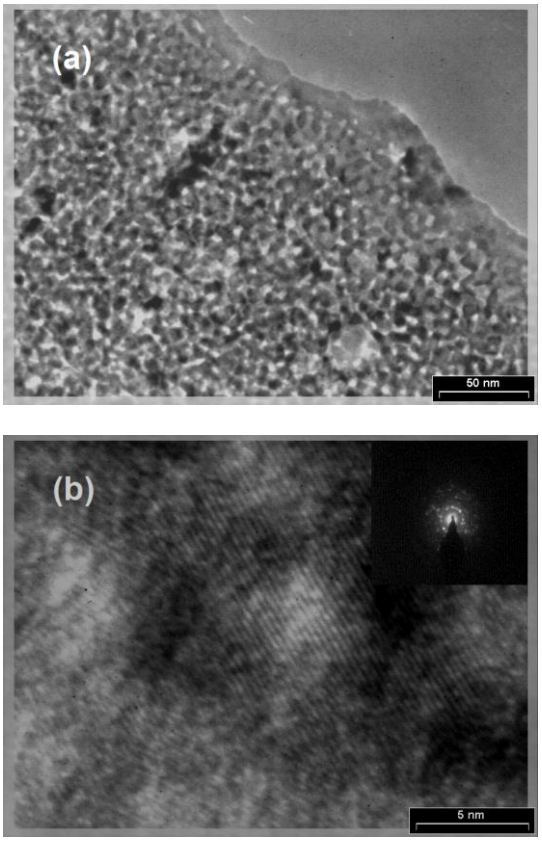

Fig. 4. TEM images of the continual mesoporous TiO_2 film annealed at 400 ℃ with two magnifications (a) and (b), the inset is a selected area electron diffractogram of the sample.

3.4. Optical characterization

The transmittance spectra of continual mesoporous TiO_2 films annealed at different temperatures are shown in Fig. 5. All films exhibit good transmittance (up to 80 %) in the visible region and a sharp fall in the UV region, which corresponds to the band gap. It can be observed that by increasing temperature, transmittance maxima decreases and the absorption edges shift to a longer wavelength. These changes are significantly considerable at 700 °C mainly due to the phase transition from anatase to rutile phase as observable in the X-ray diffraction patterns. The optical band gap (Eg) in a semiconductor is determined by Tauc's equation [18]:

$$\alpha = \frac{k\left(h\upsilon - E_g\right)^n}{h\upsilon}$$

where α is optical absorption coefficient, k is a constant, hν is the photon energy (eV) and n may have different values like 1/2, 2, 3/2 or 3 for allowed direct and indirect and forbidden direct and indirect transitions, respectively [19]. The optical band gap is estimated by extrapolating the straight-line portion of the $(\alpha h\nu)^{1/2}$ vs. hν plot. Fig. 6 shows the change in optical band gap with the annealing temperature. The band gap of the film annealed at 300 °C is 3.61 eV and it gradually decreases to 3.43 eV after annealing at 700 °C. The decrease in the optical band gap of the continual mesoporous TiO_2 films with the annealing temperature might be a result of the change in film density, increase in crystallite sizes and anatase to rutile phase transition. The observed values are higher than the band gap of both bulk and thin film TiO_2. The larger band gap of the film in comparison to their bulk values is contributed to the lattice deformation by an axial strain. The higher band gap observed in our case can be due to the quantum size effects arising from the small size of TiO_2 nano crystallites present in the continual mesoporous film [20].

3.5. Photovoltaic performance of DSSCs

Anatse phase because of its high electron mobility and low dielectric constant has a better influence on the photovoltaic performance of DSSCs compared to other phases [5]. Therefore, the effect of annealing temperature was studied in temperature range of 400 to 600 °C which the anatase phase can be stable. The photocurrent density-voltage (J-V) characteristics of DSSCs made of continual mesoporous TiO_2 films with different annealing temperatures and film thicknesses are illustrated in Fig. 7. In addition, the corresponding photovoltaic parameters such as short circuit current (Jsc), open circuit voltage (V_{OC}), fill factor (FF) and power conversion efficiency (η) are summarized in Table 2. It can be observed that with the increase of deposition cycles from 4 to 12, the film thickness increased from 0.7 to 2.0 μm at constant annealing temperature of 400 °C. By increasing film

thickness from 0.7 to 1.7 μm, the short circuit current increases from 2.59 to 8.05 mA/cm^2 but when it reaches to 2.0 μm, the short circuit current decreases to 7.57 mA/cm^2.

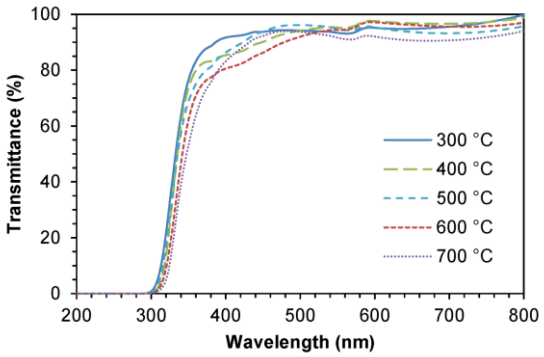

Fig. 5. Optical transmittance spectra of the continual mesoporous TiO_2 films annealed at different temperatures.

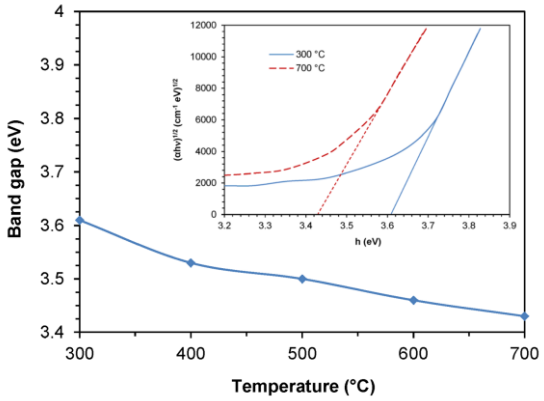

Fig. 6. Optical band gap estimated for continual mesoporous TiO_2 films annealed at different temperatures, the inset is the plot of $(\alpha h\nu)^{1/2}$ vs. $h\nu$.

The open circuit voltage increases from 0.701 to 0.761 V as the films thickness increases. Cells conversion efficiency is affected by the changes of the short circuit current. A film with a 0.7 μm thickness, which is the least amount, has the minimum power conversion efficiency of 0.98 % and the maximum power conversion efficiency of 3.61 %, is obtained in optimum film thickness of 1.7 μm. Increasing the short circuit current in solar cells with film thickness less than 1.7 μm resulted from the increase of films specific surface area. By increasing the number of deposition cycles, films specific surface area increased and resulted in adsorbing more dye molecules to the surface which as a result increases the density of TiO_2 conduction band electrons. But in the films which have more than 1.7 μm thicknesses, because of increasing recombination centers resulted from the increase in films thickness, the amount of reduction of oxidized electrolyte carriers with injected electrons to TiO_2 conduction band increased and consequently decreased the short circuit current. Besides, there is a possibility that with the increase of deposition cycles, the surface area becomes less due to the elimination the surface area of bottom layers as a result of annealing. Thus the increase of thickness up to the optimum level has increased the cells conversion efficiency [21]. The open circuit voltage mainly depends upon the quasi Fermi level of TiO_2 conduction band and redox potential of electrolyte. Fermi level is a function of electrons density and trapping centers. Their changes with increasing film thickness enhance the value of open circuit voltage [22].

Also, it is found that when the annealing temperature of films with the same thickness increases from 400 to 600 °C, both the short circuit current and open circuit voltage decreased from 8.05 to 6.77 mA/cm^2 and 0.761 to 0.736 V, respectively. Therefore, the power conversion efficiency decreases to 2.94 % by increasing annealing temperature to 600 °C. The power conversion efficiency changes based on annealing temperature is affected by the changes in structural, optical and surface properties of the films. As the XRD results show, increasing annealing temperature results in crystallites growth and decreases lattice strain of anatase phase which explains the reduction of electron trapping centers such as defects and crystallite boundaries. With reducing these inhibitors, the electrons scattering becomes lower and their diffusion coefficient becomes higher which improve charge collection efficiency. The increases of light absorption in the visible region and shifts the absorption edge of the films towards longer wavelength increased the density of injected electrons to TiO_2's conduction band and also the charge injection efficiency. However, according to the results of surface area analysis, if annealing temperature becomes 200 °C higher, the films specific surface area will be about 46 % lower, which has led to a huge drop in the amount of up taked dye molecules and also in the light harvest efficiency. Decline in the short circuit current because of annealing temperature increase shows that the reduction of specific surface area has much stronger effect on lowering the injected electrons to TiO_2's conduction band compared to the other two improving factors [21, 23]. As it was mentioned the open circuit voltage is a function of the electrons density in conduction band of TiO_2 films, so higher electrons density by increasing annealing temperature decreased the value of open circuit voltage [22].

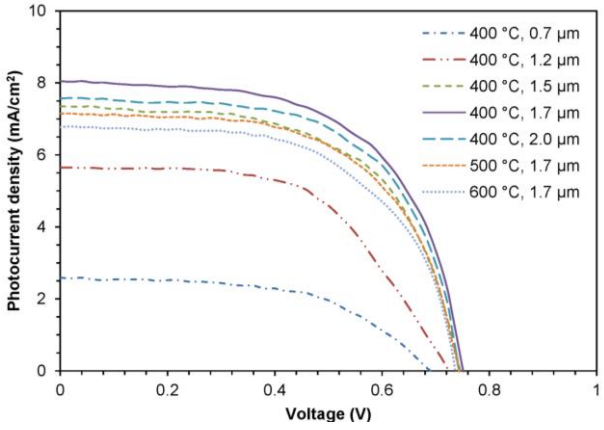

Fig. 7. Photocurrent density-voltage curves of DSSCs made of continual mesoporous TiO_2 films in different annealing temperatures and thicknesses.

Table 2. Photovoltaic parameters of DSSCs made of continual mesoporous TiO_2 films in different annealing temperatures and thicknesses.

Deposition cycles	Thickness (μm)	Annealing temperature (°C)	J_{SC} (mA/cm^2)	V_{OC} (V)	FF	η (%)
4	0.7	400	2.59	0.701	0.54	0.98
6	1.2	400	5.65	0.733	0.56	2.31
8	1.5	400	7.35	0.749	0.59	3.25
10	1.7	400	8.05	0.761	0.59	3.61
12	2.0	400	7.57	0.760	0.60	3.45
10	1.7	500	7.15	0.743	0.60	3.19
10	1.7	600	6.77	0.736	0.59	2.94

4. Conclusions

Dye-sensitized solar cells (DSSCs) based on continual mesoporous TiO_2 films were successfully fabricated by sol-gel spin coating tempelating technique. The effects of annealing temperature and film thickness were examined on the photovoltaic performance of solar cells. XRD-results showed that anatase phase crystallized at 300 °C with crystallite size of 3.2 nm and transformed to rutile phase at 700 °C. Anatase phase was under tensile strain, and the strain decreased by increasing the annealing temperature. The specific surface area of the films annealed at 400 °C was 163.43 m^2/g and decreased to 87.15 m^2/g at 700 °C. TEM images proved the nanostructured and continual mesoporous morphology of TiO_2 deposited films. As the temperature increased, the transmittance maxima of the films decreased in the visible region and the absorption edges shifted to longer wavelengths. The estimated optical band gap of the films decreased from 3.61 to 3.43 eV by increasing the annealing temperature from 300 to 700 °C. The film with the optimum thickness of 1.7 μm obtained the maximum power conversion efficiency of 3.61 %. This power conversion efficiency decreased to 2.94 % with enhancement of the annealing temperature to 600 °C.

References

[1] B. O'Regan, M. Gratzel, Nature **353**, 737 (1991).
[2] J. Gong, J. Liang, K. Sumathy, Ren, Sus Ene Rev **16**, 5848 (2012).
[3] M. Gratzel, Inorg. Chem. **44**, 6841 (2005).
[4] P. Hsiao, K. Wang, C. Cheng, H. Teng, Photochem and Photobio A: Chem **188**, 19 (2007).
[5] T. K. Yuna, S. S. Park, D. Kim, Y. Hwang, S. Huh, J. Y. Bae, Y. S. Won, J Pow Sour **196**, 3678 (2011).
[6] S. L. Chung, C. M. Wang, J Mater Sci & Tech **28**, 713 (2012).
[7] D. H. Cha, Y. S. Kim, J. H. Pan, Y. H. Lee, W. I. Lee, Stud Surf Sci Catal **165**, 625 (2007).
[8] S. Ngamsinlapasathian, S. Pavasupree, Y. Suzuki, S. Yoshikawa, Sol Ene Mater & Sol Cel **90**, 3187 (2006).
[9] J. M. Szeifert, D. Fattakhova-Rohlfing, D. Georgiadou, V. Kalousek, J. Rathousky, D. Kuang, S. Wenger, S. M. Zakeeraddin, M. Gratzel, T. Bein, Chem Mater **21**, 1260 (2009).
[10] Y. Fu, Z. Jin, Y. Ni, H. Du, T. Wang, Thin Solid Films **517**, 5634 (2009).
[11] H. Yun, K. Miyazawa, I. Honma, H. Zhou, M. Kuwabara, Mater Sci and Eng **C 23**, 487 (2003).
[12] K. Liu, M. Zhang, K. Shi, H. Fu, Mater Lett **59**, 3308 (2005).
[13] C. J. Brinker, Y. Lu, A. Sellinger, H. Fan, Adv Mater **11**, 579 (1999).
[14] P. Yang, D. Zhao, D. I. Margolese, B. F. Chmelka, G. D. Stucky, Nature **396**, 152 (1998).
[15] B. D. Cullity, Elements of X-ray diffraction, Addison-Wesley, London (1978).
[16] H. Tang, F. Levy, H. Berger, P. E. Schmid, Phys Rev **B 52**, 7771 (1995).
[17] M. Wark, J. Tschirch, O. Bartels, D. Bahnemann, J. Rathousky, Micropor Mesopor Mater **84**, 247 (2005).
[18] M. Sreemany, S. Sen, Mater Chem and Phys **83**, 169 (2004).
[19] D. Bhattacharyya, S. Chaudhuri, A. K. Pal, Vacuum **43**, 313 (1992).
[20] H. C. Ong, A. X. E. Zhu, Appl Phys Lett **80**, 941 (2002).
[21] J. Prochazka, L. Kavan, V. Shklover, M. Zukalova, O. Frank, M. Kalbac, A. Zukal, H. Pelouchova, P. Janda, K. Mocek, M. Klementova, D. Carbone, Chem Mater **20**, 2985 (2008).
[22] E. J. W. Crossland, M. Nedelcu, C. Ducatic, S. Ludwigs, M. A. Hillmyer, U. H. Steiner, J. Snaith, Nano lett **9**, 2813 (2009).
[23] P. Balraju, P. Suresh, M. Kumar, M. S. Roy, G. D. Sharma, J Photochem Photobiol A: Chem **206**, 53 (2009).

*Corresponding author: byarmand@merc.ac.ir